Journal of Sustainable Energy & Environment

11 (2020) 81-91

Evaluation of multiple sub-daily satellite precipitation products for Thailand

Hoang Thi Trang[1,2], Kasemsan Manomaiphiboon[1,2,*], Nkrintra Singhrattna[3], Nosha Assareh[1,2]

[1]The Joint Graduate School of Energy and Environment, King Mongkut's University of Technology Thonburi, Thailand
[2]Center of Excellence on Energy Technology and Environment, Ministry of Higher Education, Science, Research, and Innovation, Thailand
[3]Department of Public Works and Town and Country Planning, Bangkok, Thailand
*Corresponding author: kasemsan_m@jgsee.kmutt.ac.th, Tel.: +66 2 470-7331

Abstract: This study assessed the prediction performance of seven satellite precipitation products using the 3-hourly gauge data in 2014-2016 across Thailand, as the representative country in Upper Southeast Asia. They are Tropical Rainfall Measuring Mission near-real-time (TRMM_RT), gauge-adjusted TRMM (TRMM), Climate Prediction Center Morphing (CMORPH), Global Precipitation Measurement (GPM), Global Satellite Mapping of Precipitation - Standard (GSMaP_S), gauge-adjusted GSMaP (GSMaP_G), and Precipitation Estimation from Remotely Sensed Information using Artificial Neural Network (PERSIANN). The evaluation methods include bias, error, and correlation, event detection, phase of diurnality, variance partitioning, and wavelet coherence. No single product is universally superior over all aspects. Nevertheless, it is possible to suggest CMORPH as the best performing based on the majority of the methods. GPM and GSMaP_S also perform reasonably, except for incompatibility in the diurnality phase. These three products capture precipitation fluctuations to some extent, as robustly indicated by variance partitioning and wavelet coherence. GSMaP_G has the true strength in bias, error, and correlation but fails to capture the fluctuations. GSMaP_G and GPM detect the "light" class of precipitation event the best but only GPM continues to predict relatively well for the "moderate" and "heavy" classes. TRMM_RT appears to have relatively large bias and error and does not reasonably capture the fluctuations. PERSIANN has relatively large error and does not perform well for correlation and event detection.

Keywords: Rainfall, Harmonic analysis, Monsoon, Spectral decomposition, Autocorrelation.

1. Introduction

Direct precipitation measurement by conventional gauges is not only simple but generally considered standard for reference use. For certain remote areas or areas with diverse topography, complex climate patterns [33, 41, 47], gauges may not be available or only sparsely distributed, posing difficulty in knowing precipitation intensity and other related characteristics. Alternative methods, such as ground-based radar and satellite remote sensing, are helpful and applicable to such case. It is nonetheless important to understand the accuracy and uncertainty in their precipitation estimates, which are normally evaluated by comparing against gauge measurement. The ground-based radar, if available, provides information of precipitation and its propagation at relatively high spatial and temporal resolutions but its estimates are subject to various sources of error such as instrument, degraded signal, atmospheric conditions, and ground clutter [3] but may be limited in area coverage. For the satellite precipitation estimates, derived from space-based remotely sensed data and specialized algorithms, they have received much interest from both research and operational communities and are becoming advanced with time. A recent review by Kidd and Huffman (2011) [29] provides a historical background and technical perspectives of satellite-derived precipitation measurement. Several satellite precipitation products (SPPs) are currently produced at sub-daily and spatially fine (e.g., 0.25° or smaller) resolutions, with (quasi-)global coverage. Bias and error in such data intrinsically exist and depend on several factors, e.g., the hydro-climatic background of a region of interest [4, 37, 39], sensor type [23, 41], and algorithms/assumptions used in the estimation process [42]. The importance of sub-daily precipitation is generally associated with short-term weather impacts and public risks (e.g., flash floods, landslides, and transportation accidents) as well as its influence on how people plan and manage their outdoor activities (e.g., travelling, recreation, and business) [5]. Sub-daily precipitation also modulates atmospheric variables at a diurnal scale [48] (e.g., temperature, humidity, visibility, and air pollution) and is also an essential input to hydrological modeling [50]. Precipitation studies at a sub-daily scale are often constrained or limited due to lack of accessibility or availability of sub-daily data (particularly, gauge data) [54], which can alternatively be supported by SPPs [1, 18]. SPPs become indispensable in case of no or limited gauge installations. Guo et al. [18] showed fair agreement of a sub-daily SPP with gauges over Tibet and found it to be topographically dependent. Pribadi et al. (2012) [38] and Limsakul et al. (2014) [31] applied such satellite data to examine the diurnal variation of precipitation in the Indonesian Maritime Continent and Thailand, respectively.

Given SPP assessment, a relatively large number of studies focus on daily and monthly scales, such as Southern China [53], the Upper Mekong River Basin [6, 20], the Chinese mainland [39], and Malaysia [47]. In Thailand, Chokngamwong and Chiu (2008) [7] evaluated two daily Tropical Rainfall Measuring Mission (TRMM) data (version 5 and gauge-adjusted version 6) [23-24]. Janjai et al. (2015) [26] examined monthly estimates from the TRMM, the Climate Prediction Center (CPC) Morphing (CMORPH) [27], and a geostationary satellite, and reported superior performance in the first and the third. Sub-daily evaluations have received less attention, and some early studies are Dai et al. (2007) [10] and Shen et al. (2010) [43] for example. To our knowledge, no dedicated assessment on sub-daily SPPs has been conducted for the region of Upper Southeast Asia (or called the Lower Mekong River region or Indochinese Peninsula), which

has formed a motivational basis of this study. Here, we aim to assess the prediction performance of seven gridded sub-daily SPPs with gauge data in Thailand, a tropical country situated in the center of the region, by incorporating a number of conventional and non-conventional methods to describe their predictability of precipitation estimates, which include seasonal bias and error, precipitation event detection, phase of diurnality, variance partitioning using spectral decomposition, and wavelet coherence.

2. Study Area

Thailand, like most parts of Upper Southeast Asia, has a tropical climate and diverse topography. The two prevailing monsoons (southwest and northeast) mainly influence its climate [12, 49]. The southwest monsoon carries warm moist air from the Indian Ocean, bringing about precipitation for the most part of the country (i.e., the wet season). The wet season spans about May-October. The Gulf of Thailand contributes additional moisture along the passage of the monsoonal winds. The intertropical convergence zone (ITCZ) impacts precipitation at a sub-seasonal scale [35]. Tropical cyclones that develop in the North Indian and Western Pacific Ocean Basins also play a modulating role in precipitation intensity [12]. The northeast monsoon spans about November-February, bringing cool dry air from the mid-latitudes (i.e., the winter) to Upper Thailand. When the northeasterly winds pass over the Gulf of Thailand, moisture can be absorbed into air masses and intensifies precipitation along the eastern side of peninsular Lower (i.e., Southern) Thailand. March-April marks the warmest time of the year (i.e., the summer), during which the northeast monsoon weakens greatly [44]. In the following, the wet and dry seasons defined correspond to the months May-October and November-April, respectively. Climatologically, the wet season contributes as much as 80% of annual precipitation over the entire Thailand [49]. Such seasonal contrast in precipitation amount is also revealed by GAUGE, as seen in Figure 1b.

3. Data and Methods

3.1 SPPs

The first two SPPs (out of seven) considered are TRMM version 7, produced by the National Aeronautics and Space Administration (NASA) and the Japan Aerospace Exploration Agency (JAXA) (available at ftp://trmmopen.gsfc.nasa.gov): TRMM near-real-time 3B42RT (shortly, TRMM_RT) and TRMM post-real-time 3B42 (shortly, TRMM), both of which provide relatively long-term data (since 1 January 1998) with 0.25° and 3-hourly resolutions. These products were combined from multi precipitation estimates from microwave (MW) and infrared (IR) sensors from various satellites [23-24]. It is noted that the TRMM (3B42) product is generated from TRMM_RT (3B42RT) merged with monthly gauge data.

The third SPP is CMORPH, produced by the National Oceanic and Atmospheric Administration (NOAA) and the CPC [27]. CMORPH has a long-term data archive, starting from 1 January 1998. Precipitation estimation makes use of a morphing technique, by which MW estimates together with their features are spatially propagated and interpolated using motion vectors given by IR data. Gauge and ground-based radar data over the United State and gauge data in Australia were used to calibrate final estimates. CMORPH offers various datasets with different grid and temporal resolutions, and the specific product adopted here is of version 1, with 0.25° and 3-hourly resolutions (available at ftp://ftp.cpc.ncep.noaa.gov/precip/CMORPH_V1.0/RAW/0.25deg-3HLY).

The fourth SPP is Global Precipitation Measurement (GPM) version 6, developed by the NASA and the JAXA [21, 25, 45]. The GPM mission is a direct successor to the TRMM mission and makes use of a constellation of satellites, with the GPM Core Observatory being the core satellite of the GPM constellation and having two major sensors (GPM Microwave Imager or GMI and Dual-frequency Precipitation Radar or DPR) on board. Among several levels of data products, the gridded level-3 of the Integrated Multi-Satellite Retrievals for GPM (IMERG) products are commonly used by researchers and operational workers. Specifically, the GPM product considered in this study is the "Final Run" product, which has 0.1° and half-hourly resolutions. IMERG, as the unified algorithm, combines data from all passive-microwave instruments in the constellation to produce precipitation estimates. It is noted that the product used here has been adjusted to the monthly Global Precipitation Climatology Project (GPCP) Satellite-Gauge product over high-latitude ocean and tropical land and to the seasonal GPCP Satellite-Gauge surface precipitation data to correct known biases. The availability of the used GPM product begins from June 2000 (available at ftp://jsimpson.pps.eosdis.nasa.gov/NRTPUB/imerg/late).

The next two SPPs are Global Satellite Mapping of Precipitation (GSMaP) version 6 [17, 32, 52] (available at ftp://rainmap@hokusai.eorc.jaxa.jp/reanalysis/v6). GSMaP is a scientific project initialized by the Japan Science and Technology Agency and later supported by the JAXA Precipitation Measuring Mission (PMM) Science Team. Three main products are available: standard (GSMaP_S), gauge-adjusted (GSMaP_G), and near-real-time (GSMaP_NRT). The precipitation estimation is based on combing MW, IR, and DPR data from various sensors, using two main algorithms (microwave radiometer and blended-microwave-infrared). Here, the non-near-real time products (i.e., GSMaP_S and GSMAP_G) were considered, and both have 0.1° and hourly resolutions. The main difference is that GSMaP_G is derived from GSMaP_S with daily gauge adjustment.

The last SPP is Precipitation Estimation from Remotely Sensed Information Using Artificial Neural Network (PERSIANN), developed by the Center for Hydrometeorology and Remote Sensing (CHRS) [22, 46]. Its precipitation estimates are derived from IR brightness temperature imagery provided by geostationary satellites and artificial neural network (ANN) procedures, with MW data used to calibrate IR-based estimates. The finest spatial and temporal resolutions given by PERSIANN are 0.25° and 3-hourly, respectively, spanning from 1 February 2000, which were considered here (available at ftp://persiann.eng.uci.edu/CHRSdata/PERSIANN/3hrly). The sensors used and associated data incorporated for each of SPPs are listed in Table S1 of Supplementary Materials.

3.2 Gauge data

Three-hourly precipitation data at 105 gauges of the Thai Meteorological Department (TMD) were used for the evaluation against the SPPs. These selected gauges are officially registered by the World Meteorological Organization (WMO) (Supplementary Materials, Table S2), and their recordings are internally quality-checked before public distribution. The gauge data available to and used by us span three years (2014-2016), report accumulated amount at 01, 04, 07, …, 19, and 22 LT (LT = UTC + 7), and have high adequacy (≥99% of total records at every gauge). To have a common basis for all gridded SPPs, a grid of a 0.25° resolution was adopted as a reference to support the evaluation (here, compatible with the TRMM grid). After overlaying the gauges onto the grid, the gauges are fully covered by 93 grid cells (81 with a single gauge, and 12 with double gauges inside) (Figure 1a). At any grid cell with double gauges, its representative latitude/longitude values and precipitation were assigned as the averages over the two gauges. These 93 grid cells are to be hereafter referred to as sites. As seen, they are fairly distributed over Thailand, with elevations of 0-400 m msl (above

mean sea level) based on the ASTER Global Digital Elevation Model (ASTER GDEM) data version 2 (with a product resolution of 30 m) [2]. The gauged data used in the evaluation will be referred to shortly as GAUGE. The Thiessen-polygon area of each site was determined and used as a weight in area-wide averaging.

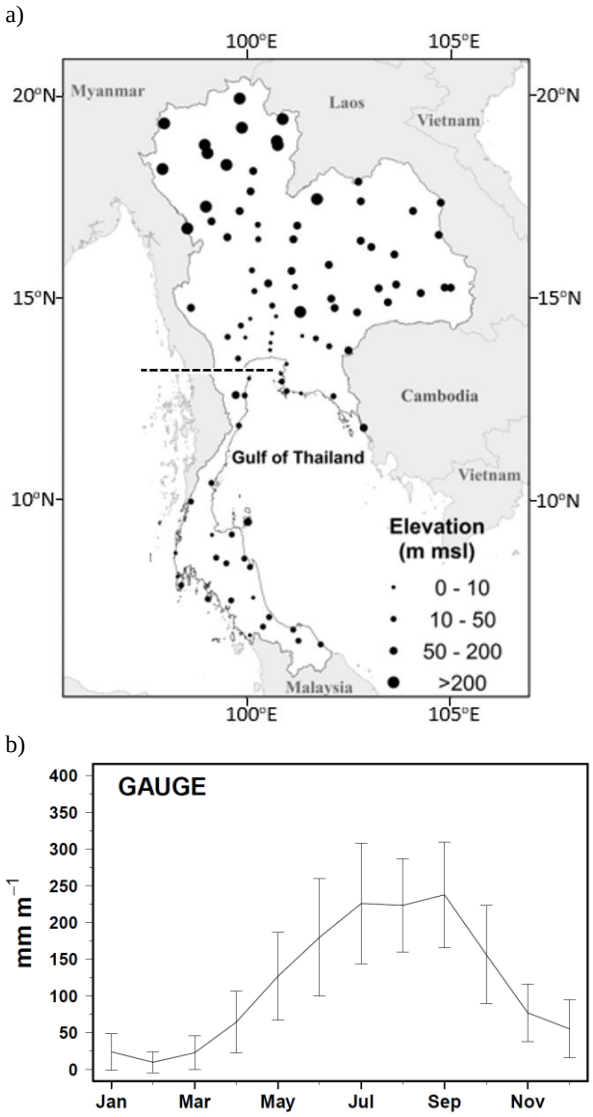

Figure 1. (a) Thailand and 93 gauge sites. Lower or Southern Thailand generally refers to the peninsular part while Upper Thailand is the remaining part (as seen divided by the horizontal dashed line) and (b) Observed monthly area-average precipitation based on the 3-year period. The vertical lines denote standard deviation. The wet season (May-Oct) accounts for 83% of total annual amount.

3.3 Precipitation classes

To detect precipitation events, four classes were defined, which are none (<0.1 mm $3h^{-1}$ as no rain or trace), light (≥0.1 mm $3h^{-1}$ and ≤5 mm $3h^{-1}$), moderate (>5 mm $3h^{-1}$ and ≤15 mm $3h^{-1}$), and heavy (>15 mm $3h^{-1}$). Given no standard 3-hourly thresholds of the light/moderate and moderate/heavy classes officially used in Thailand, simple quantile matching was here applied to scale from the TMD's standard daily thresholds (http://www.tmd.go.th/met_dict.php). In doing so, daily data were first prepared from 3-hourly data at each gauge site. For each of the two thresholds, the probability of the daily threshold was computed and then used to inversely determine the corresponding 3-hourly precipitation. The threshold was approximately assigned as the median of all precipitation values from all sites in question. It was found that the probabilities found at the light/moderate threshold are between 0.43 and 0.77, with the median of 0.68. For the moderate/heavy threshold, the range is between 0.75 and 0.97, with the median of 0.92, which is reasonably high to represent heavy precipitation. Based on GAUGE, the occurrences of the four precipitation classes are about 90% (none), 7% (light), 2% (moderate), and 1% (heavy) (see Figure S1 of Supplementary Materials).

3.4 SPP data preparation

The SPPs in question may have different choices of time in reporting accumulated precipitation. It was found that CMORPH, GPM, GSMaP_G, GSMaP_S, and PERSIANN use the concept of "report at the starting time". For example, 3-hourly data reported at 0600 UTC correspond to observation over 0600-0859 UTC. Both TRMM and TRMM_RT use the middle-time convention, e.g., data at 0600 UTC corresponds to observation over 0430-0729 UTC. However, GAUGE uses the ending-time convention, the SPP data were adjusted or linearly interpolated to be consistent with that of GAUGE. The SPPs may also have different grid configurations (cell alignment and spacing). They were, if necessary, re-gridded to follow the 0.25° reference grid (as stated in Section 3.2), using overlapping-area-weighted averaging. It is noted that the focal resolution in the current study is 0.25°, which is the same as TRMM, TRMM_RT, CMORPH, and PERSIANN, but the native spacing of the remaining SPPs (i.e., GPM, GSMaP_S, and GSMaP_G) is 0.1°. Thus, the assessment of the 0.1° data was included and discussed but in a limited fashion.

3.5 Methods

We begin to describe the SPP evaluation using the following three conventional metrics: normalized mean bias (NMB), normalized mean error (NME), and Pearson correlation (r). The definitions of NMB and NME are as follows:

$$\text{NMB}\ (\%) = \frac{1}{N\,\bar{O}} \sum_{i=1}^{N} (P_i - O_i) \times 100 \tag{1}$$

and

$$\text{NME}\ (\%) = \frac{1}{N\,\bar{O}} \sum_{i=1}^{N} |P_i - O_i| \times 100, \tag{2}$$

where O_i is the i^{th} observation, P_i is the corresponding i^{th} prediction, $\bar{O}$ is the average of observation, and N is the number of data pairs. Negative NMB reflects underestimation or dry bias, while positive NMB corresponds to overestimation or wet bias. The closer NMB or NME to zero, the better performance.

To assess how well a SPP detects precipitation events, three metrics were adopted for use here, which are hit rate (HR), false alarm rate (FAR), and false negative rate (FNR). HR is the ratio of events when both observation and prediction fall within the same specified class. FAR is the ratio of events with prediction found in a higher class than observation, and vice versa for FNR. According to these definitions, the sum of HR, FAR, and FNR equals unity for each class. Each of these metrics has a range between 0 and 1, with 1 as the best score for HR but 0 as the best score for FAR and FNR.

To evaluate the diurnal cycle of precipitation, a harmonic analysis [1, 10, 55] was performed, which mathematically expresses the diurnal cycle as

$$y_t = \bar{y} + \sum_{k=1}^{n/2} \left\{ C_k \cos\left(\frac{2\pi k t}{n} - \phi_k \right) \right\}, \tag{3}$$

where $\bar{y}$ is the mean of the series, t is the hour of day (here, 3-hourly), n is the period of one cycle (equal to 24), k is the order of harmonic, C_k is the amplitude of the k^{th} harmonic, and ϕ_k is the phase of the k^{th} harmonic which corresponds to the peak-amplitude time of the cycle. The above equation can be algebraically rearranged into [55, see pages 371-378 therein]

$$y_t = \bar{y} + A_1 \cos\left(\frac{2\pi t}{n}\right) + B_1 \sin\left(\frac{2\pi t}{n}\right) + A_2 \cos\left(\frac{2\pi 2t}{n}\right) + B_2 \sin\left(\frac{2\pi 2t}{n}\right) + \ldots + A_k \cos\left(\frac{2\pi kt}{n}\right) + B_k \sin\left(\frac{2\pi kt}{n}\right) \quad (4)$$

with $A_k = C_k \cos(\phi_k)$, $B_k = C_k \sin(\phi_k)$, and $C_k = A_k^2 + B_k^2$. Only the wet season was considered because precipitation is concentrated during this season, enabling robust harmonic fitting. In the fitting, the average diurnal cycle at each site was used, normalized to zero mean and unit standard deviation. The normalization helps remove bias effects on the amplitude and also facilitates phase comparison. Multiple linear regression can be used for fitting based on the above equation, giving the values of coefficients A_1, B_1, A_2, B_2, …, A_k, and B_k and then those of C_k and ϕ_k. It was found that using only the first- and second-order harmonics (shortly, the 1st and 2nd harmonics, i.e., $k \le 2$) combined adequately explains the total variance in the original cycle (here, >80% for over three quarters of all sites). Our visual inspection generally found a fair-to-good fit (Figure S5 in Supplementary Materials). In the evaluation, two metrics were employed, which are phase bias (PB) and phase error (PE). Their formulas are given as follows:

$$\mathrm{PB} = (\theta_{p,i} - \theta_{o,i})_{\mathrm{dir}} \quad (5)$$

and

$$\mathrm{PE} = \left|\theta_{p,i} - \theta_{o,i}\right|_{\mathrm{dir}}, \quad (6)$$

where $\theta_{o,i}$ and $\theta_{p,i}$ are the observed and predicted i^{th} phases, respectively, whose values are assigned as zero at the north axis and increase clockwise from the axis, and the subtraction operation is directional, as denoted by subscript "dir" in the above equations. Both PB and PE have the same unit of decimal degree (here, 360° is equivalent to 24 hours). It should be noted that the 1st-harmonic phase has only one single value while the 2nd-harmonic phase has two values (separated by 180°). Before computing PB and PE, the values of any pair of observed and predicted phases are directionally aligned to be within 180°. Negative PB (i.e., negatively shifted) occurs when the predicted phase lags behind the observed phase, and vice versa for positive bias (i.e., positively shifted).

Variability is an important aspect of precipitation. In this study, precipitation variability is described based on a spectral approach. In general, a climatic time series comprises superimposed fluctuations at many time scales (from sub-daily or intra-day to multi-year scales), driven by micro/meso/synoptic processes, disturbances, and large-scale teleconnections. It is of interest to determine how total variability in precipitation data is explained by different temporal scales. Variance is essentially a statistical measure of variability in data. Eskridge et al. (1997) [11] developed a variance partitioning technique using Kolmogorov-Zurbenko (KZ) filters, by which the total variance of original data is decomposed into those pertaining to different temporal scales. A recent review of the KZ filtering and its applications was given by Yang and Zurbenko (2010) [56]. In this study, the spectral decomposition using KZ filters were applied to find the decomposed variances of each SPP in order to be compared later with those of GAUGE, similar to Torsri et al. (2013) [51] where those of regional climate model output and those of observational data were compared. In general, the KZ technique has relatively clean filtering (with suitable filter parameters) and permits missing values in the calculation. By definition, KZ(m, p) is a long-pass filter that operates as a p-time iterative of a moving average with length m [11]:

$$y(t) = \frac{1}{m} \sum_{i=-(m-1)/2}^{(m-1)/2} x(t+i), \quad (7)$$

where m is an odd integer (≥3) and p is an integer (≥1). In the iteration, $y(t)$ from the first iteration becomes the input for the second iteration and so on, until the p^{th} iteration. Here, the original time series, denoted by $x(t)$, can be written as

$$x(t) = \mathrm{ID}(t) + \mathrm{SB}(t) + \mathrm{SY}(t) + \mathrm{LT}(t), \quad (8)$$

where the right-hand-side terms are the decomposed components at the intra-day (or sub-daily), sub-seasonal (or synoptic), seasonal-to-year, and long-term scales, respectively. To filter out fluctuations with cycles of N time steps or less (here, 3 hours per step), m and p are required to follow $m \times p^{1/2} \le N$.

For each dataset, the following filters were sequentially applied to obtain the time series of the decomposed components individually:

a) KZ(3, 1) on the original data to remove cycles of 9 hours or less, yielding SB + SY + LT. ID simply equals x – SB – SY – LT,

b) KZ(301, 5) on the result from a) to remove cycles of 2.8 months or less, yielding SY + LT, and

c) KZ(2001, 3) on the result from b) to remove cycles of 1.2 years or less, yielding LT.

It is noted that we tried a number of different sets of (m, p), examined their corresponding transfer functions [11], and finally found the above-specified filters technically applicable. The degree of separation among the decomposed components was also inspected by comparing the sum of variances from these individual components to the total variance of the original data (the closer, better the separation).

The spectral analysis using the KZ filtering is technically constrained to the frequency domain. However, whether the degree of compatibility of spectral power (or variance) between GAUGE and each SPP still holds or varies in a time domain should be addressed. In doing so, wavelet coherence was utilized. Wavelet is a spectral technique to delineate the oscillations or fluctuations of a time series in both time and frequency domains simultaneously, and wavelet coherence is a measure of how correlated a pair of time series are in terms of oscillation power. The wavelet-based techniques have been applied to help interpret the information or features of climate variability [13-16, 34]. Here, the "biwavelet" library on the R platform [15] was used to compute squared wavelet coherence between the GAUGE and SPP series. Its value ranges between 0 and 1 (the larger value, the higher correlation). In our calculation setup, the standard "Morlet" mother wavelet function was employed, as suggested in Grinsted et al. (2004) [16]. Any missing values with no more than two consecutive records were filled by linear interpolation; otherwise, they were zero-padded.

4. Results and discussion

4.1 Bias, error, and correlation

In both dry and wet seasons, TRMM_RT, TRMM, and GPM show wet bias against GAUGE while the others yield dry bias, except for CMORPH and GSMaP_G whose bias turns out to change direction from the dry bias in the wet season to the wet bias in the dry season (Table 1). Wet bias by TRMM-based SPPs were also reported in other studies, e.g., Khan et al. (2014) [28] for Pakistan, Qin et al. (2014) [39] for China, Satgé et al. (2016) [41] for the Andean Plateau, and Tan et al. (2015) [47] for Malaysia. In Li et al. (2019) [30], wet bias was also reported in TRMM (version 7) and GPM (versions 3, 4, and 5) over a hydrological basin in Thailand, with equal or larger magnitudes in the latter. Here, GPM (version 6) appears to improve with lower wet bias in the wet season and both seasons combined. In both seasons combined, TRMM and GSMaP_G have the least bias in magnitude (<12%) possibly because both are gauge-adjusted. Gauge adjustment has the potential to reduce the magnitude of bias substantially [43, 19]. As for NME, its value ranges 112%-150% across the SPPs and seasons, being relatively low in CMORPH and GSMaP_S but relatively high in TRMM_RT. Comparing between TRMM_RT and TRMM, the latter (as gauge-adjusted) performs better in all three metrics (NMB, NME, and *r*). GSMaP_G (as gauge-adjusted) shows the least bias in magnitude and highest correlation in magnitude in all cases. However, the gauge adjustment in GSMaP_G does not offer less error with respect to its counterpart (GSMaP_S). All SPPs are fairly correlated to GAUGE ($r = 0.3$-0.5), with the highest values found in GSMaP_G and GPM and the lowest values in PERSIANN. No drastic changes in correlation among the seasons were found. In view of spatial distribution (Figures S2-S4 in Supplementary Materials), GPM shows the most apparent seasonal contrast in NMB, especially in Upper Thailand while the other SPPs have less seasonal contrast. For NME, the majority of the sites register >100% values in both dry and wet seasons, and none registers <50%. In both seasons, every SPP has the majority of the sites registered with fair correlation (0.3-0.6), except for PERSIANN having low correlation (<0.3) for most sites. Dry-season GSMaP_G has about one-third of the sites with high correlation (>0.6).

As mentioned previously, each of GPM, GSMaP_S, and GSMaP_G has a native finer resolution (0.1°). Whether the above evaluation results (based on the 0.25° resolution) would hold with the finer resolution is also of interest. We examined this aspect and found no systematic and substantial impacts on the three metrics for these three SPPs (Table 1). That is, NMB and NME change in magnitude within 3% and 6%, respectively, and correlation is still maintained at 0.4-0.5. Moreover, we assessed the SPP performance with increasing averaging time (Figure 2). Bias is theoretically unaffected because the averaging is a linear process and only error and correlation are relevant, as suggested in Conti et al. (2014) [8]. As seen in every SPP, NME and correlation improve relatively fast during the 3-hour to 6-hour averaging times and continue to improve but with a slower rate, suggesting the 6-hourly time scale as a challenging threshold to the sub-daily SPPs and their performance. Notice that, towards the 24-hour averaging time, GSMaP_G is the best SPP, which is due possibly to daily gauge adjustment. The final aspect of the evaluation described in this section is whether the SPP performance depends on gauge elevation. Here, four elevation intervals (0-10, 10-50, 50-200, and >200 m msl) were defined (Figure 1), and their corresponding number of gauge sites are 16, 31, 32, and 14 sites, respectively. TRMM and GPM do not show elevation dependence in both bias and error (Figure 3) whereas the other SPPs have mixed or incoherent results. GSMaP_G shows a wet-to-dry shift over the first two intervals and a dry-to-wet over

Table 1. Area-average normalized mean bias, and normalized mean error, and correlation found in each SPP. All results are based on the reference 0.25° resolution, except for those in the cases of GPM, GSMaP_S, and GSMaP_G where the results based on their native 0.1° resolutions are additionally shown in parentheses.

Dataset	Quantity	Both seasons	Wet	Dry
Gauge	Mean±SD (mm 3h^{-1})	0.5±3.1	0.8±3.9	0.2±1.7
TRMM_RT	Mean±SD (mm 3h^{-1})	0.6±2.4	0.9±2.9	0.2±1.4
	NMB (%)	26.4	27.4	21.4
	NME (%)	149.3	150.0	143.5
	r	0.42	0.40	0.40
TRMM	Mean±SD (mm 3h^{-1})	0.5±2.1	0.8±2.6	0.2±1.2
	NMB (%)	9.2	11.4	6.6
	NME (%)	136.1	137.8	129.4
	r	0.43	0.41	0.43
CMORPH	Mean±SD (mm 3h^{-1})	0.4±2.0	0.6±2.4	0.2±1.4
	NMB (%)	−14.6	−17.2	6.4
	NME (%)	120.0	118.6	127.8
	r	0.43	0.42	0.44
GPM	Mean±SD (mm 3h^{-1})	0.5±2.1 (0.5±2.4)	0.8±2.5 (0.8±2.9)	0.2±1.4 (0.2±1.6)
	NMB (%)	7.5 (8.2)	3.3 (4.2)	43.3 (45.5)
	NME (%)	125.5 (125.6)	122.4 (121.7)	147.7 (153.8)
	r	0.50 (0.49)	0.49 (0.49)	0.49 (0.44)
GSMaP_S	Mean±SD (mm 3h^{-1})	0.4±1.8 (0.4±1.9)	0.6±2.1 (0.6±2.3)	0.2±1.2 (0.2±1.2)
	NMB (%)	−18.2 (−18.6)	−18.1 (−18.1)	−17.5 (−18.5)
	NME (%)	121.2 (117.1)	122.5 (118.4)	111.5 (108.8)
	r	0.41 (0.44)	0.38 (0.42)	0.45 (0.47)
GSMaP_G	Mean±SD (mm 3h^{-1})	0.5±1.4 (0.5±1.5)	0.8±1.7 (0.8±1.8)	0.2±0.8 (0.2±0.8)
	NMB (%)	−1.0 (−1.2)	0.2 (0.1)	−0.3 (−0.7)
	NME (%)	130.7 (128.1)	131.7 (128.8)	127.4 (126.2)
	r	0.51 (0.53)	0.49 (0.51)	0.54 (0.55)
PERSIANN	Mean±SD (mm 3h^{-1})	0.4±1.7	0.6±2.0	0.2±1.1
	NMB (%)	−13.7	−13.9	−4.4
	NME (%)	140.2	140.6	139.7
	r	0.30	0.28	0.30

the last two intervals. Some studies (e.g., [4, 18]) but over larger ranges of elevation (e.g., several hundreds to a few thousands of meter) reported strong dependence. In our study, the highest site is located at just 400 m msl, and nearly all sites are in plains (e.g., low-lying, coastal, highland, and mountain-valley), as opposed to on mountains or hills, and this may possibly not allow us to capture or reveal the influence of elevation clearly, which is a limitation of the current study.

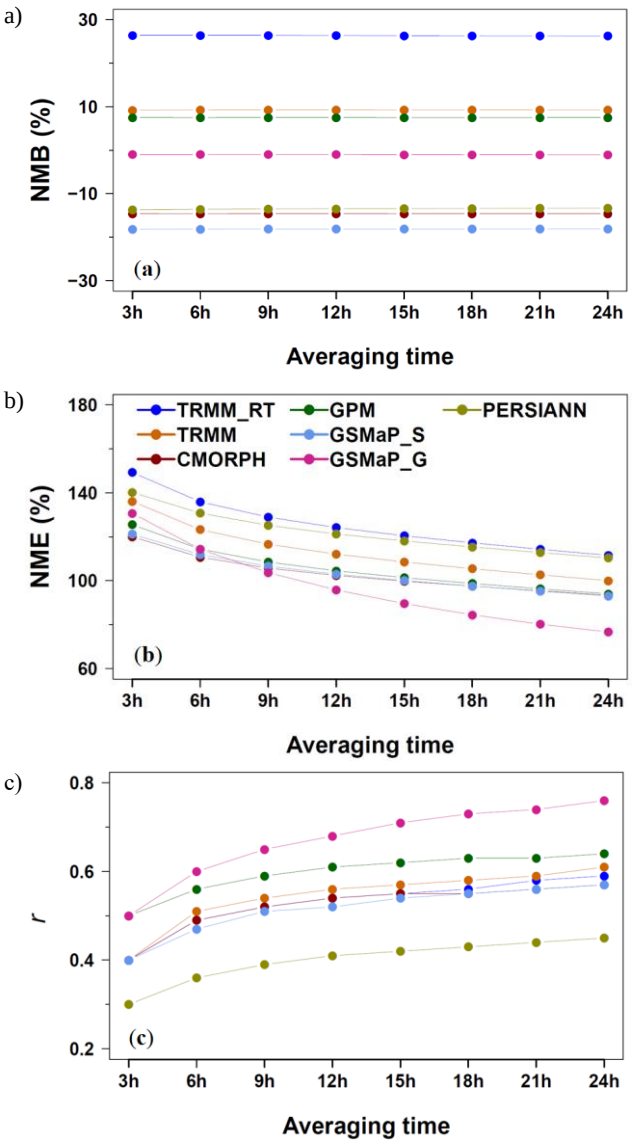

Figure 2. Change with averaging time of (a) normalized mean bias, (b) normalized mean error, and (c) correlation for both dry and wet seasons combined.

4.2 Precipitation event detection

Following the four defined classes of precipitation events (none, light, moderate, and heavy) for the precipitation event detection, it was found that all SPPs commonly predict the "none" class well and the "light" class fairly (HR $\geq$ 0.4) but relatively poor for the other two classes (HR $\leq$ 0.3) (Figure 4). The difficulty of detecting heavy-precipitation events was also reported in Chokngamwong and Chiu (2008) [7] and Prakash et al. (2018) [37]. The overall findings from the current assessment are as follows: In view of HR, both GSMaP_G and GPM detect the "light" class the best but the "none" class the worst. However, GPM still persists to perform relatively well for the two upper classes ("moderate" and "heavy"), as opposed to GSMaP_G that

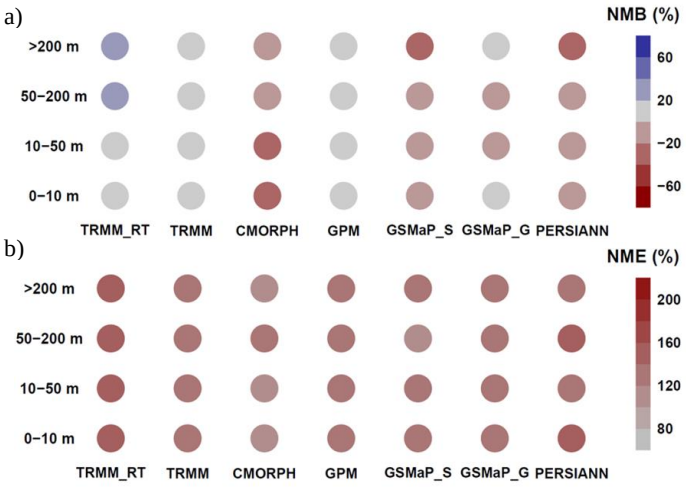

Figure 3. Change with surface elevation (m msl) of (a) normalized mean bias and (b) normalized mean error for both dry and wet seasons combined.

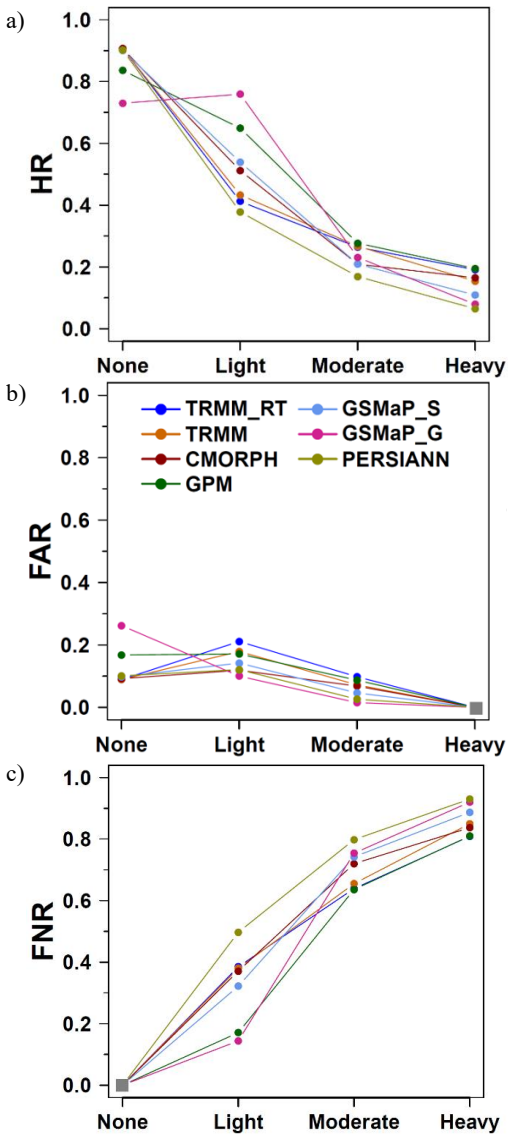

Figure 4. (a) Hit rate, (b) false alarm rate, and (c) false negative rate by precipitation class for both dry and wet seasons combined. The grey solid squares in (b) and (c) indicate no calculation.

yields relatively poor detection in the "heavy" class. It is known that several technical enhancements were made in the GPM mission, as compared to the TRMM mission, and a notable one is the GPM precipitation radar and sensors having more sensitivity to light precipitation [53]. The SPPs generally have low FAR (<0.3) in every class but high FNR (>0.6) in the two upper classes. TRMM_RT gives false alarm the most often in the "light" and "moderate" classes. PERSIANN may be viewed as the worst-performing, particularly from the viewpoint of HR and FNR.

4.3 Phase of diurnality

For the 1st harmonic, every SPP shows only a positive phase shift (PB = 2.1-20.4°, equivalent to 0.1-1.4 hours preceding) while, for the 2nd harmonic, phase shifts both negatively and positively (PB = –10.3° to 20.4°) (Table 2). CMORPH appears to perform the best in both 1st-and 2nd-harmonics, followed by TRMM and TRMM_RT. GSMaP_S and GPM yield the largest PB and PE in the 1st harmonic. Figure 5 illustrates the spatial distribution of the 1st- and 2nd-harmonic phases for GAUGE and two examples of SPPs (CMORPH and GSMaP_S as well- and poorly-performing, respectively) (see Figures S6-S7 in Supplementary Materials for all SPPs). It is worth noting from the figures that the 1st-harmonic phase of GAUGE varies spatially but tends to fall in the evening hours over the most of Upper Thailand but in the afternoon in Lower Thailand (Figure 5). Wet-season precipitation in Bangkok (the capital) mostly peaks in the late afternoon, evening, and early morning, depending on the month, as a result of the delayed effect of surface heating by the sun [5]. Maximum precipitation occurs in the evening or nighttime at the coastal sites in the eastern part of Thailand and some sites near the northeastern border to Laos, as similarly reported by Ohsawa et al. (2001) [36] for June-August precipitation in Thailand.

Table 2. Area-average phase bias and phase error for the 1st and 2nd harmonics. Units are decimal degree (360° = 24 hours).

SPP	1st Harmonic		2nd Harmonic	
	PB (deg.)	PE (deg.)	PB (deg.)	PE (deg.)
TRMM_RT	9.7	25.8	4.6	22.4
TRMM	9.3	24.3	4.0	20.5
CMORPH	2.1	17.9	1.7	15.1
GPM	15.5	23.1	9.7	15.4
GSMaP_S	20.4	33.0	9.9	28.4
GSMaP_G	9.3	30.6	–10.3	35.0
PERSIANN	8.1	33.0	20.4	23.6

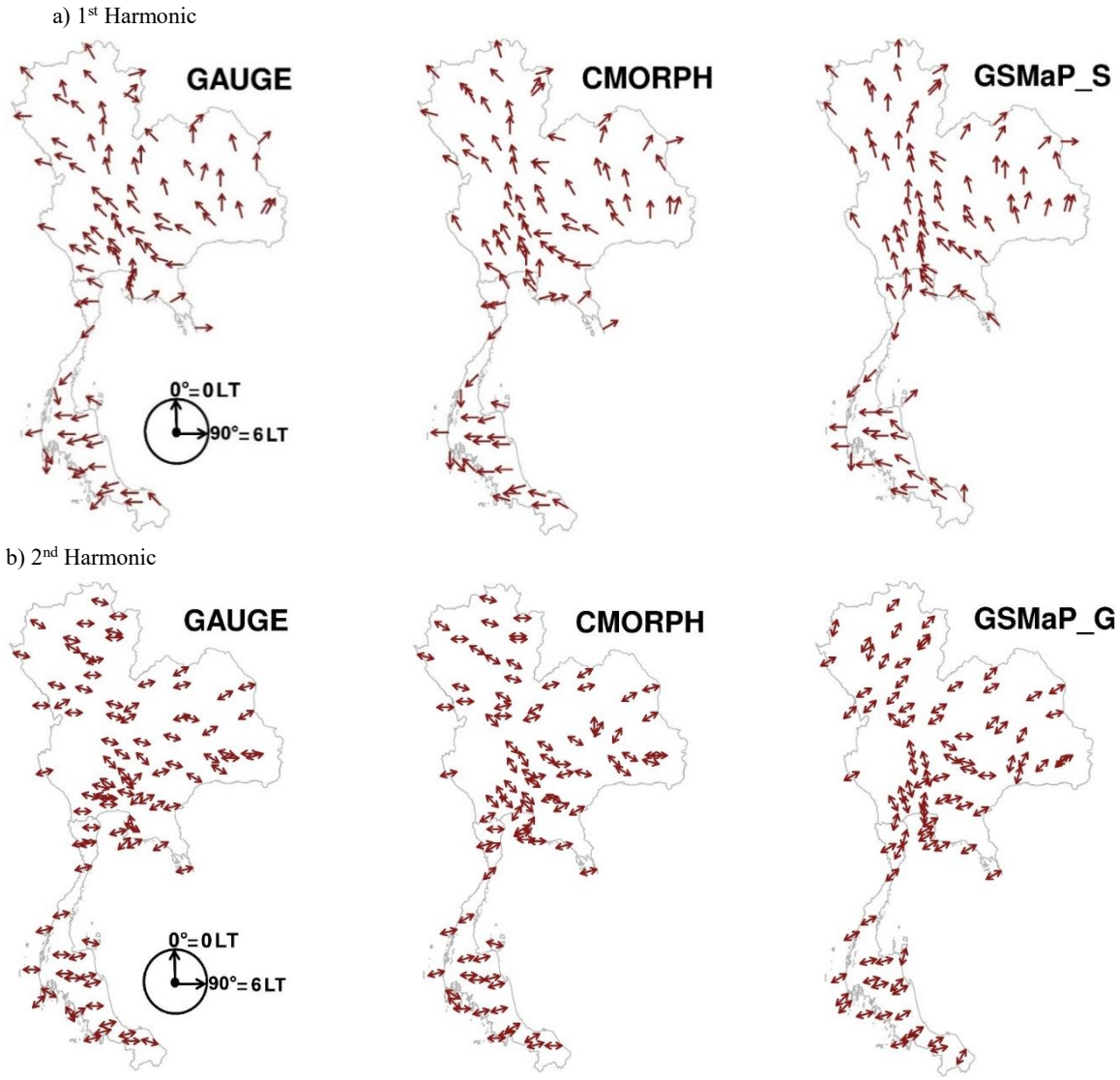

Figure 5. Phase vectors of wet-season-only precipitation by GAUGE, CMORPH, and GSMaP_S. The single- and double-headed arrows correspond to the peak-amplitude times of the 1st and 2nd harmonics, respectively.

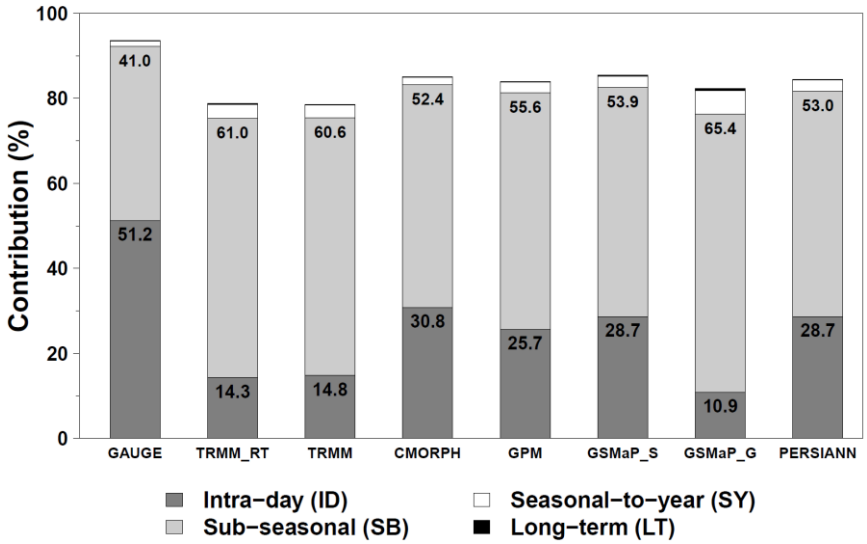

Figure 6. Variance contribution (relative to total variance) from each temporal component of precipitation in both dry and wet seasons combined.

4.4 Variance partitioning

A fair-to-good separation (>78% of the total variance) was achieved in each of GAUGE and the SPPs (Figure 6). For GAUGE, most of its total variance (93.6%) is explained by the ID, SB, SY, and LT variances combined (51.2%, 41.0%, 1.3%, and 0.1%, respectively). Every SPP under-predicts in the ID variance (20-40%) but over-predicts the SB variance by 11-24%. Among all SPPs, CMORPH, followed by GSMaP_S, GPM, and PERSIANN shows better performance in capturing the decomposed variances, relatively close to those given by GAUGE. TRMM_RT, TRMM, and GSMaP_G are identified as the least performing ones. In addition to the above spectral results, we examined the autocorrelation of 3-hourly precipitation (Figure 7a). Autocorrelation is a basic property of a stochastic process that is tightly associated with how the process evolves with time based on its past states [9].

From the figure, it decays rapidly with time lag for every dataset. CMORPH is shown to yield the shape of the autocorrelation closet to that of GAUGE. As seen, GAUGE has a decorrelation time (marked by the e-folding or the 1/e value) of 2.3 hours. For CMORPH, GPM, GSMaP_S and, PERSIANN, the decorrelation time is slightly longer (3.6 hours) while the remaining SPPs have many prolonged times (4.7-6.6 hours), the latter of which may be explained by the influence of larger-scale fluctuations (especially, the overestimated variance of the SB component). We also further examined zero-time-lag correlation but with distance separation (Figure 7b), similarly finding CMORPH to be superior among all SPPs, with its decorrelation distance of about 80 km, closest to that of GAUGE (about 30 km).

4.5 Wavelet coherence

The results of wavelet coherence over the cycles of <48 hours are only displayed because the sub-daily scale is of most interest (Figure 8). Given the 3-hourly data, results at the cycles of <6 hours were necessarily omitted to avoid the effect of aliasing [55]. In general, wavelet coherence varies with time with seasonal contrast in a pattern. That is, every SPP shows pronounced coherence in the dry season due to relatively limited precipitation commonly given by all SPPs. Both CMORPH and GSMaP_S are shown to be the best, followed by GPM, based on coherence averaged over the cycles of 6-12 hours (as sub-daily-scale oscillations), which are about 0.6 for both seasons and 0.5 for the wet season alone. For the least-performing SPPs, they are TRMM_RT, TRMM, and GSMaP_G. These results are well consistent with those previously said in the previous section. Notice that, between GSMaP_S and GSMaP_G, the latter is superior at the cycles of 24-48 hours due possibly to its daily-gauge adjustment.

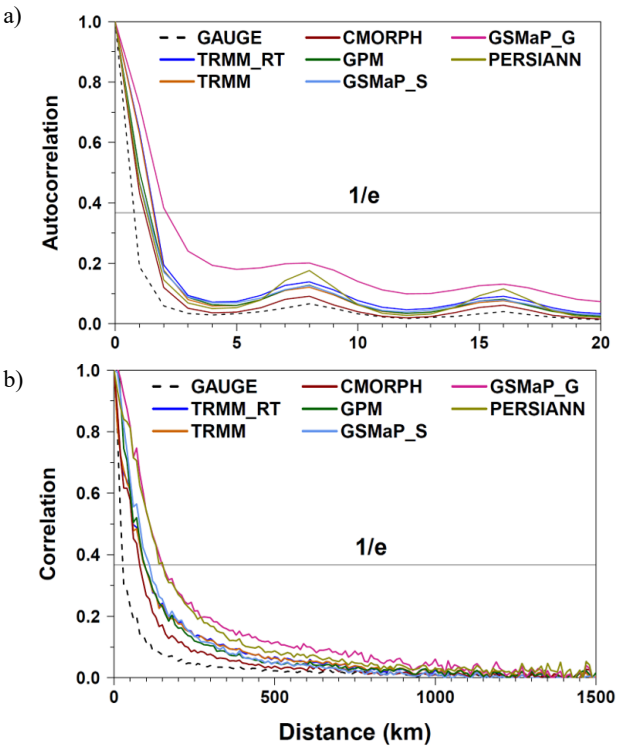

Figure 7. (a) Autocorrelation and (b) correlation with distance separation of precipitation in both dry and wet seasons combined. In each plot, the e-folding (1/e) is denoted by the horizontal grey line. For (b), correlation between each pair of sites was first computed and then grouped into 10-km distance bins. After that, all correlation results from all pairs were averaged bin-wise, in which no Thiessen-polygon-area weights were used.

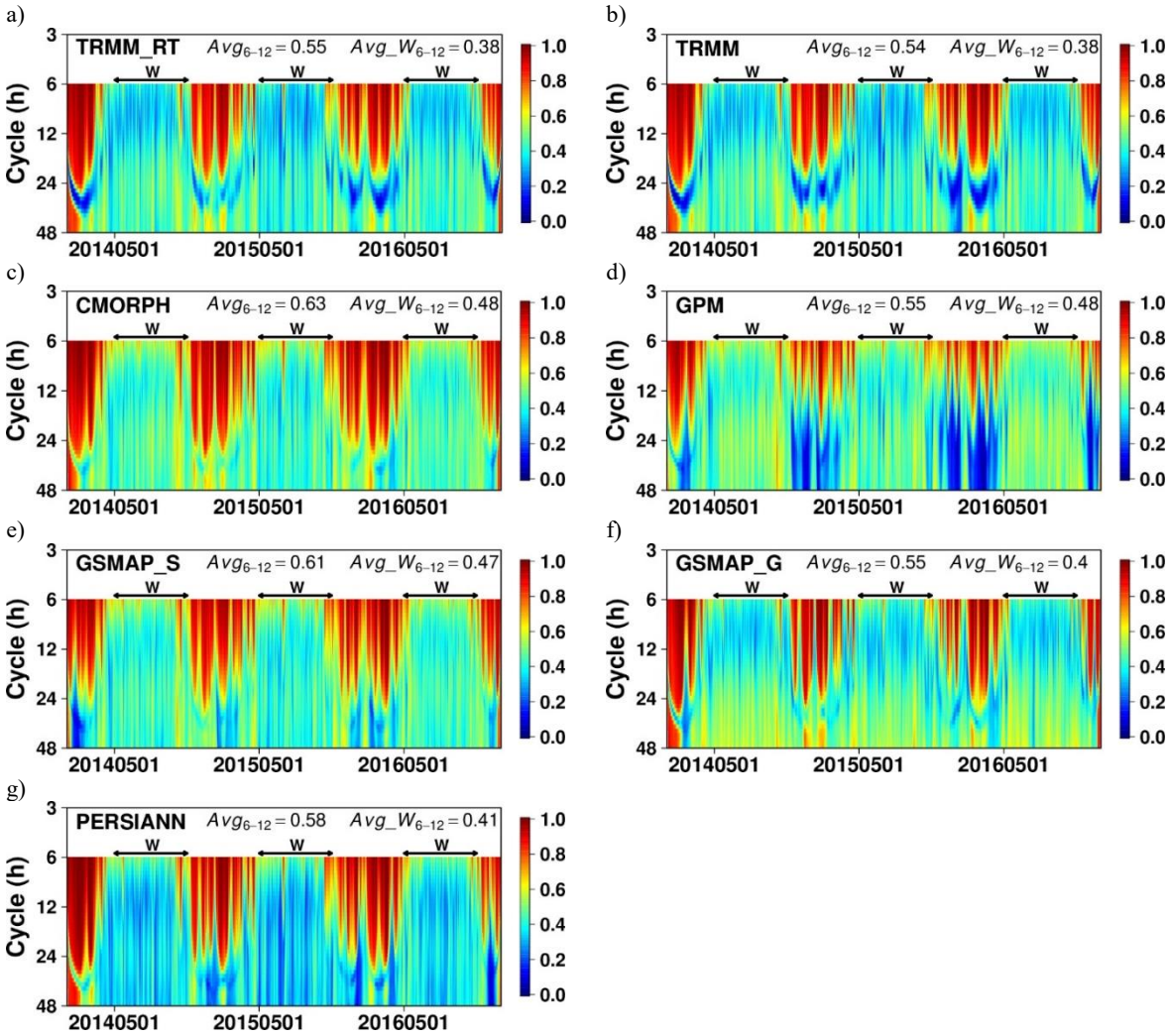

Figure 8. Squared wavelet coherence (dimensionless) between GAUGE and each SPP. Each color pixel in the above plots corresponds to the average over the same pixels pooled from all sites with Thiessen-polygon-area weights. "**W**" stands for wet season (May-October). It is noted that $Avg_{6\text{-}12}$ and $Avg\_W_{6\text{-}12}$ are the average coherence average values for only cycles of 6-12 hours in both seasons combined and wet season, respectively.

5. Conclusions

A total of seven satellite precipitation products, which are TRMM_RT, TRMM, CMORPH, GPM, GSMaP_S, GSMaP_G, and PERSIANN, have been evaluated against the 3-hourly gauge data in 2014-2016 across Thailand, as the representative tropical country in Upper Southeast Asia. The evaluation methods include bias, error, correlation, and precipitation event detection, which are conventional. The non-conventional methods utilized are phase of diurnality, variance partitioning using spectral decomposition and wavelet coherence. None of the SPPs were found to be universally superior in every aspect. It is possible to suggest CMORPH among the SPPs as the best performing based on the majority of the methods used. GPM and GSMaP_S are the noteworthy products that also perform reasonably, except only for lack of compatibility in the phase of diurnality. These three products are capable of dynamically capturing precipitation fluctuations to a certain degree, as consistently indicated by variance partitioning and wavelet coherence as well as time/space correlations. GSMaP_G has the true strength in bias, error, and correlation but fails to capture the fluctuations. Both GSMaP_G and GPM detect the "light" class the best but the "none" class the worst but GPM continues to predict relatively well for the "moderate" and "heavy" classes. TRMM_RT and PERSIANN appear to be the least favored products. The former is associated with relatively large bias and error and poorly accounting for the fluctuations whereas the latter is inferior in error, correlation, and event detection. It was also noted that bias and error do not show a strong dependence on elevation but based on the gauges used, which are still limited in height.

It is hoped that the evaluation and findings in this study can potentially provide useful information about SPP choices in terms of strengths and weaknesses and their applicability for the region in question. We nevertheless caution against directly extending the findings without further evaluation of other regions. Given the limitations and scope of the current study, some recommended future studies are the use of sub-daily gauge and satellite-based data over a longer-term period, hydrologically based evaluation during fast flood events [30], use of an independent gauge network (if accessible, especially, the inclusion of gauges located on mountains), and incorporation of additional statistical concepts, e.g., joint space-time evolution, frequency-duration characteristics, and extreme value analysis.

Acknowledgements

The authors sincerely thank the Thai Meteorological Department for the gauge data and the developers of the satellite precipitation products used in the study. We thank Dr. Penwadee Chewapongpun and Dr. Sombat Chuenchooklin for their useful

suggestions. We also thank the anonymous reviewers for their useful comments. This study was financially supported mainly by the Joint Graduate School of Energy and Environment and the Postgraduate Education and Research Development Office, and partly by the Asahi Glass Foundation, the National Research Council of Thailand, and the Hydro-Informatics Institute (Public Organization).

Supplementary Materials

The supplement information of this article is available at http://www.jseejournal.com/.

References

[1] Angelis, C.F., McGregor, G.R. and Kidd, C. 2004. Diurnal cycle of rainfall over the Amazon Basin, *Climate Research*, 26, 139-149.

[2] ASTER GDEM. 2011. *ASTER GDEM (version 2) - summary of validation results*. ASTER Global Digital Elevation Model Validation Team, Available online: https://ssl.jspacesystems.or.jp/ersdac/GDEM/ver2Validation/Summary_GDEM2_validation_report_final.pdf [Accessed on: 20 March 2020].

[3] Berne, A. and Krajewski, W.F. 2013. Radar for hydrology: Unfulfilled promise or unrecognized potential, *Advances in Water Resources*, 51, 357-366.

[4] Bharti, V. and Singh, C. 2015. Evaluation of error in TRMM 3B42V7 precipitation estimates over the Himalayan region, *Journal of Geophysical Research: Atmospheres*, 120, 12458-12473.

[5] Buajitti, K. 1960. Diurnal variation of rainfall at Bangkok, *Journal of the National Research Council of Thailand*, 1, 1-19.

[6] Chen, C.-J., Senarath, S.U.S., Dima-West, L.M. and Marcella, M.P. 2016. Evaluation and restructuring of gridded precipitation data over the Greater Mekong Subregion, *International Journal of Climatology*, 37, 180-196.

[7] Chokngamwong, R. and Chiu, L.S. 2008. Thailand daily rainfall and comparison with TRMM products, *Journal of Hydrometeorology*, 9, 256-266.

[8] Conti, F.L., Hsu, K-L., Noto, L.V. and Sorooshian, S. 2014. Evaluation and comparison of satellite precipitation estimates with reference to a local area in the Mediterranean Sea, *Atmospheric Research*, 138, 189-204.

[9] Cryer, J.D. and Chan, K. 2008. *Time Series Analysis: With Applications in R*, New York: Springer Science+Business Media, LLC, 2nd ed., 491 pp.

[10] Dai, A., Lin, X. and Hsu, K.-L. 2007. The frequency, intensity, and diurnal cycle of precipitation in surface and satellite observations over low- and mid-latitudes, *Climate Dynamics*, 29, 727-744.

[11] Eskridge, R.E., Ku, J.Y., Rao, S.T., Porter, P.S. and Zurbenko, I.G. 1997. Separating different scales of motion in time series of meteorological variables, *Bulletin of the American Meteorological Society*, 78, 1473-1483.

[12] Eso, M., Kuning, M. and Chuai-Aree, S. 2015. Analysis of daily rainfall during 2001-2012 in Thailand, *Songklanakarin Journal of Science and Technology*, 37, 81-88.

[13] Fu, G., Yu, J., Yu, X., Ouyang, R., Zhang, Y., Wang, P., Liu, W. and Min, L. 2013. Temporal variation of extreme rainfall events in China, 1961-2009, *Journal of Hydrometeorology*, 487, 48-59.

[14] Ghil, M., Allen, M.R., Dettinger, M.D., Ide, K., Kondrashov, D., Mann, M.E., Robertson, A.W., Saunders, A., Tian, Y., Varadi, F. and Yiou, P. 2002. Advanced spectral methods for climatic time series, *Reviews of Geophysics*, 1, 1003-1043.

[15] Gouhier, T.C., Grinsted, A. and Simko, V. 2019. *Package "biwavelet" version 0.20.19*, Available online: https://cran.r-project.org/web/packages/biwavelet/ [Accessed on: 20 March 2020].

[16] Grinsted, A., Moore, J.C. and Jevrejeva, S. 2004. Application of the cross wavelet transform and wavelet coherence to geophysical time series, *Nonlinear Processes in Geophysics*, 11, 561-566.

[17] GSMaP. 2014. Global Satellite Mapping of Precipitation (GSMaP) for GPM. Available online: https://www.eorc.jaxa.jp/GPM/doc/algorithm/GSMaPforGPM_20140902_E.pdf [Accessed on: 20 March 2020].

[18] Guo, J., Zhai, P., Wu, L., Cribb, M., Li, Z., Ma, Z., Wang, F., Chu, D., Wang, P. and Zhang, J. 2014. Diurnal variation and the influential factors of precipitation from surface and satellite measurements in Tibet, *International Journal of Climatology*, 34, 2940-2956.

[19] Guo, H., Chen, S., Bao, A., Hu, J., Yang, B. and Stepanian, P.M. 2016. Comprehensive evaluation of high-resolution satellite-based precipitation products over China, *Atmosphere*, 7, 6.

[20] He, Z., Yang, L., Tian, F., Ni, G., Hou, A. and Lu, H. 2017. Inter-comparisons of rainfall estimates from TRMM and GPM multi-satellite products over the Upper Mekong River Basin, *Journal of Hydrometeorology*, 18, 413-430.

[21] Hou, A.Y., Kakar, R.K., Neeck, S., Azarbarzin, A.A., Kummerow, C.D., Kojima, M., Oki, R., Nakamura, K. and Iguchi, T. 2014. The global precipitation measurement mission, *Bulletin of the American Meteorological Society*, 95, 701-722.

[22] Hsu, K.L., Gao, X., Sorooshian, S. and Gupta, H.V. 1997. Precipitation estimation from remotely sensed information using artificial neural networks, *Journal of Applied Meteorology*, 36, 1176-1190.

[23] Huffman, G.J., Adler, R.F., Bolvin, D.T., Nelkin, E.J., Bowman, K.P., Hong, Y., Stocker, E.F. and Wolff, D.B. 2007. The TRMM Multisatellite Precipitation Analysis (TMPA): quasi-global, multiyear, combined-sensor precipitation estimates at fine scales, *Journal of Hydrometeorology*, 8, 38-55.

[24] Huffman, G.J. and Bolvin, D.T. 2015. *TRMM and other data precipitation data set documentation*, Available online: https://pmm.nasa.gov/sites/default/files/document_files/3B42_3B43_doc_V7.pdf [Accessed on: 20 March 2020].

[25] Huffman, G.J., Stocker, E.F., Bolvin, D.T., Nelkin, E.J. and Tan, J. 2019. *GPM IMERG Final Precipitation L3 Half Hourly 0.1 degree×0.1 degree V06, Greenbelt, MD, Goddard Earth Sciences Data and Information Services Center (GES DISC)*, Available online: https://disc.gsfc.nasa.gov/datasets/GPM_3IMERGDF_06/summary [Accessed on: 20 March 2020].

[26] Janjai, S., Nimnuan, P., Nunez, M., Buntoung, S. and Cao, J. 2015. An assessment of three satellite-based precipitation data sets as applied to the Thailand region, *Physical Geography*, 36, 282-304.

[27] Joyce, R.J., Janowiak, J.E., Arkin, P.A. and Xie, P. 2004. CMORPH: A method that produces global precipitation estimates from passive microwave and infrared data at high spatial and temporal resolution, *Journal of Hydrometeorology*, 5, 487-503.

[28] Khan, S.I., Hong, Y., Gourley, J.J., Khattak, M.U.K., Yong, B. and Vergara, H.J. 2014. Evaluation of three high-resolution satellite precipitation estimates: Potential for monsoon monitoring over Pakistan, *Advances in Space Research*, 54, 670-684.

[29] Kidd, C. and Huffman, G. 2011. Review global precipitation measurement, *Meteorological Applications*, 18, 334-353.
[30] Li, R., Shi, J., Ji, D., Zhao, T., Plermkamon, V., Moukomla, S., Kuntiyawichai, K. and Kruasilp, J. 2019. Evaluation and hydrological application of TRMM and GPM precipitation products in a tropical monsoon basin of Thailand, *Water*, 11, 818.
[31] Limsakul, A., Humphries, U., Wangwongchai, A., Chitsuphaphan, T. and Wongwises, P. 2014. Diurnal variations in summer monsoon precipitation over Thailand and its vicinity observed from ten years of TRMM data, *Journal of Sustainable Energy and Environment*, 5, 13-19.
[32] Mega, T., Ushio, U., Kubota, T., Kachi, M., Aonashi, K. and Shige, S. 2014. Gauge Adjusted Global Satellite Mapping of Precipitation (GSMaP Gauge), *Proceedings of the XXXIth URSI General Assembly and Scientific Symposium (URSI GASS)*, Beijing, China, 16-23 August 2014, Available online: http://www.isac.cnr.it/~ipwg/meetings/tsukuba-2014/posters/P1-11_Mega.pdf [Accessed on: 20 March 2020].
[33] Mekis, E., Donaldson, N., Reid, J., Zucconi, A., Hoover, J., Li, Q., Nitu, R. and Melo, S. 2018. An overview of surface-based precipitation observations at environment and climate change Canada, *Atmosphere-Ocean*, 56, 71-95.
[34] Morozova, A.L. and Barlyaeva, T.V. 2016. The role of climatic forcing in variations of Portuguese temperature: A comparison of spectral and statistical methods, *Journal of Atmospheric and Solar-Terrestrial Physics*, 149, 240-257.
[35] Octaviani, M. and Manomaiphiboon, K. 2011. Performance of regional climate model RegCM3 over Thailand, *Climate Research*, 47, 171-186.
[36] Ohsawa, T., Ueda, H., Hayashi, T., Watanabe, A. and Matsumoto, J. 2001. Diurnal variations of convective activity and rainfall in tropical Asia, *Journal of the Meteorological Society of Japan*, 79, 333-352.
[37] Prakash, S., Mitra, A.K., AghaKouchak, A., Liu, Z., Norouzi, H. and Pai, D.S. 2018. A preliminary assessment of GPM-based multi-satellite precipitation estimates over a monsoon dominated region, *Journal of Hydrology*, 556, 865-876.
[38] Pribadi, A., Wongwises, P., Humphries, U., Limsakul, A. and Wangwongchai, A. 2012. Diurnal rainfall variation over three rainfall regions within Indonesia based on ten years of TRMM data, *Journal of Sustainable Energy and Environment*, 3, 81-86.
[39] Qin, Y., Chen, Z., Shen, Y., Zhang, S. and Shi, R. 2014. Evaluation of satellite rainfall estimates over the Chinese mainland, *Remote Sensing*, 6, 11649-11672.
[40] R Development Core Team. 2019. *The R Project for Statistical Computing (version 3.6.0)*.
[41] Satgé, F., Bonnet, M.-P., Gosset, M., Molina, J., Lima, W.H.Y., Zolá, R.P., Timouk, F. and Garnier, J. 2016. Assessment of satellite rainfall products over the Andean Plateau, *Atmospheric Research*, 167, 1-14.
[42] Scofield, R.A. and Kuligowski, R.J. 2003. Status and outlook of operational satellite precipitation algorithms for extreme-precipitation events, *Weather and Forecasting*, 18, 1037-1051.
[43] Shen, Y., Xiong, A., Wang, Y. and Xie, P. 2010. Performance of high-resolution satellite precipitation products over China, *Journal of Geophysical Research: Atmospheres*, 115, D02114.
[44] Singhrattna, N., Rajagopalan, B., Kumar, K.K. and Clark, M. 2005. Inter-annual and inter-decadal variability of Thailand summer monsoon season, *Journal of Climate*, 18, 1697-1708.
[45] Skofronick-Jackson, G., Petersen, W.A., Berg, W., Kidd, C., Stocker, E.F., Kirschbaum, D.B., Kakar, R., Braun, S.A., Huffman, G.J., Iguchi, T., Kirstetter, P.E., Kummerow, C., Meneghini, R., Oki, R., Olson, W.S., Takayabu, Y.N., Furukawa, K. and Wilheit, T. 2017. The Global Precipitation Measurement (GPM) mission for science and society, *Bulletin of the American Meteorological Society*, 98, 1679-1695.
[46] Sorooshian, S., Hsu, K.L., Gao, X., Gupta, H.V., Imam, B. and Braithwaite, D. 2000. Evaluation of PERSIANN system satellite-based estimates of tropical rainfall, *Bulletin of the American Meteorological Society*, 81, 2035-2046.
[47] Tan, M.L., Ibrahim, A.L., Duan, Z., Cracknell, A.P. and Chaplot, V. 2015. Evaluation of six high-resolution satellite and ground-based precipitation products over Malaysia, *Remote Sensing*, 7, 1504-1528.
[48] Thornes, J., Bloss, W., Bouzarovski, S., Cai, X., Chapman, L., Clark, J., Dessai, S., Du, S., der Horst, D.v., Kendall, M., Kidd, C. and Randalls, S. 2010. Communicating the value of atmospheric services, *Meteorological Applications*, 17, 243-250.
[49] TMD. 2019. *Climate of Thailand*. Thai Meteorological Department, Available online: https://www.tmd.go.th/en/archive/thailand_climate.pdf [Accessed on: 20 March 2020].
[50] Todd, M.C., Barrett, E.C., Beaumont, M.J. and Bellerby, T.J. 1999. Estimation of daily rainfall over the upper Nile river basin using a continuously calibrated satellite infrared technique, *Meteorological Applications*, 6, 201-210.
[51] Torsri, K., Octaviani, M., Manomaiphiboon, K. and Towprayoon, S. 2013. Regional mean and variability characteristics of temperature and precipitation over Thailand in 1961-2000 by a regional, *Theoretical and Applied Climatology*, 113, 289-304.
[52] Ushio, T., Sasashige, K., Kubota, T., Shige, S., Okamoto, K., Aonashi, K., Inoue, T., Takahashi, N., Iguchi, T., Kachi, M., Oki, R., Morimoto, T. and Kawasaki, Z.I. 2009. A Kalman filter approach to the Global Satellite Mapping of Precipitation (GSMaP) from combined passive microwave and infrared radiometric data, *Journal of the Meteorological Society of Japan*, 87A, 137-151.
[53] Wang, Z., Zhong, R., Lai, C. and Chen, J. 2017. Evaluation of the GPM IMERG satellite-based precipitation products and the hydrological utility, *Atmospheric Research*, 196, 151-163.
[54] Westra, S., Fowler, H.J., Evans, J.P., Alexander, L.V., Berg, P., Johnson, F., Kendon, E.J., Lenderink, G. and Roberts, N.M. 2014. Future changes to the intensity and frequency of short-duration extreme rainfall, *Reviews of Geophysics*, 52, 522-555.
[55] Wilks, D.S. 2006. *Statistical Methods in the Atmospheric Sciences*, Academic Press, 2nd ed., 648 pp.
[56] Yang, W. and Zurbenko, I.G. 2010. Kolmogorov-Zurbenko filters, *WIREs Computational Statistics*, 2, 340-351.

